AD-A048 978

PENNSYLVANIA STATE UNIV   UNIVERSITY PARK
TRANSIENT COMBUSTION IN SOLID PROPELLANT CRACKS.(U)
OCT 77   K K KUO, A T CHEN, D R MCCLURE

F/G 21/9.2

N60530-76-C-0138

NWC-TP-5943

END

CONT.

DATE
FILMED

2-78

DDC
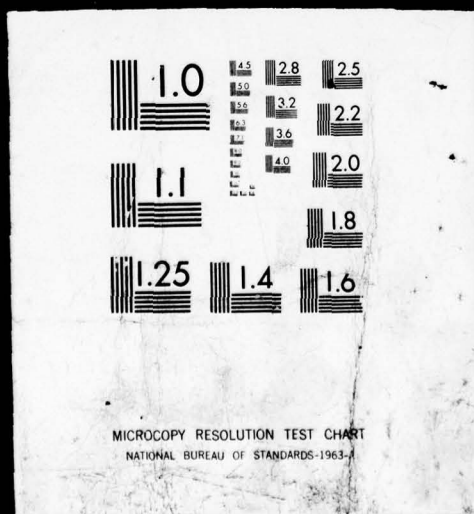
AD
A048978

MICROCOPY RESOLUTION TEST CHART
NATIONAL BUREAU OF STANDARDS-1963-A

NWC TP 5943

Transient Combustion in Solid Propellant Cracks

by
K. K. Kuo
D. R. McClure
A. T. Chen
F. G. Lucas
Pennsylvania State University
for the
Research Department

OCTOBER 1977

DDC
RECEIVED
JAN 24 1978
D

Naval Weapons Center

CHINA LAKE, CALIFORNIA 93555

Naval Weapons Center
AN ACTIVITY OF THE NAVAL MATERIAL COMMAND

SECURITY CLASSIFICATION OF THIS PAGE *(When Data Entered)*

REPORT DOCUMENTATION PAGE		READ INSTRUCTIONS BEFORE COMPLETING FORM
1. REPORT NUMBER NWC TP-5943	**2. GOVT ACCESSION NO.**	**3. RECIPIENT'S CATALOG NUMBER**
4. TITLE *(and Subtitle)* TRANSIENT COMBUSTION IN SOLID PROPELLANT CRACKS.		**5. TYPE OF REPORT & PERIOD COVERED** Research Progress Report. Jan—Dec 76
		6. PERFORMING ORG. REPORT NUMBER
7. AUTHOR(s) K. K. Kuo → A. T. Chen, D. R. McClure F. G. Lucas		**8. CONTRACT OR GRANT NUMBER(s)** N60530-76-C-0138
9. PERFORMING ORGANIZATION NAME AND ADDRESS Pennsylvania State University University Park, Pennsylvania 16802		**10. PROGRAM ELEMENT, PROJECT, TASK AREA & WORK UNIT NUMBERS** Task B0003001 B0003 001
11. CONTROLLING OFFICE NAME AND ADDRESS Naval Weapons Center China Lake, California 93555		**12. REPORT DATE** Oct 977
		13. NUMBER OF PAGES 42 / 43 p.
14. MONITORING AGENCY NAME & ADDRESS *(if different from Controlling Office)*		**15. SECURITY CLASS.** *(of this report)* UNCLASSIFIED
		15a. DECLASSIFICATION/DOWNGRADING SCHEDULE

16. DISTRIBUTION STATEMENT *(of this Report)*

Approved for public release; distribution unlimited.

17. DISTRIBUTION STATEMENT *(of the abstract entered in Block 20, if different from Report)*

18. SUPPLEMENTARY NOTES

19. KEY WORDS *(Continue on reverse side if necessary and identify by block number)*

Crack geometry   Propellant crack combustion
Combustion chamber   Transient combustion phenomena
Empirical heat transfer
Flame propagation

20. ABSTRACT *(Continue on reverse side if necessary and identify by block number)*

(See back of form.)

DD FORM 1 JAN 73 **1473** EDITION OF 1 NOV 65 IS OBSOLETE
S/N 0102-014-6601 |

SECURITY CLASSIFICATION OF THIS PAGE *(When Data Entered)*

278 650

(U) *Transient Combustion in Solid Propellant Cracks*, by K. K. Kuo, D. R. McClure, A. T. Chen, and F. G. Lucas, Pennsylvania State University. China Lake, Calif., Naval Weapons Center, October 1977, 42 pp. (NWC TP 5943, publication UNCLASSIFIED.)

(U) A one—dimensional theoretical model, incorporating the Noble-Abel dense gas law, has been developed to describe the transient model combustion phenomena inside a propellant crack. The theoretical model can be used to predict wave phenomena, heat transfer from the gas to the propellant surface and associated thermal penetration, flame propagation, and resultant pressurization at various locations along the propellant cavity.

(U) Calculations made with the current theoretical model revealed that the internal pressurization rate, pressure gradient, and flame velocity in propellant cracks (for which gases can penetrate) decrease as: the gap width increases, the rocket chamber pressurization rate decreases, and the propellant gasification temperature increases. Additionally, the predicted flame spreading was found to decelerate in a region near the crack tip; this phenomena has been experimentally observed by others.

(U) A laboratory—size combustion chamber has been designed to establish a fundamental data base in propellant crack combustion and to verify the predicative capability of the theoretical model. Preliminary experimental data, obtained in wide cracks (~0.1 cm) for relatively low chamber pressurization rates, closely compare with theoretical predictions.

D D C

RECEIVED

JAN 24 1978

D

CONTENTS

INTRODUCTION

Voids, cracks, or fissures in solid propellant grains have been responsible for the failure of many rocket motors to meet acceptance specifications.[1] These defects may originate as a result of the manufacturing process, damage received during handling and transportation, and chemical aging or thermal stresses incurred during storage. However, even though the propellant grain is crack-free before firing, there is a possibility that cracks can form in regions of large stress concentration during rocket motor operation. Combustion within a crack can lead to a pressure build-up sufficient to cause further propagation of the crack, resulting in an unexpected increase in the surface available for burning. Thus, there has been much concern among rocket motor designers as to the extent that crack combustion may contribute to catastrophic failure.

The ignition and combustion processes in solid propellant cracks generally involve:

1. Penetration of rocket chamber combustion gases into the crack cavity..

2. Convective heating of the propellant crack surface to ignition and transient conduction within the solid propellant.

3. Pressure wave phenomena in the longitudinal direction of the crack.

4. Flame spreading along the crack.

5. Cavity pressurization due to gasification of the solid propellant.

---

[1] Raytheon Company. *Storage Reliability of Missile Material Program, Solid Propellant Rocket Motor Analysis*, by D. F. Malik. Huntsville, Ala., May 1976. (Report No. LC-76-OR1 (also DDC Report AD-A026105), publication UNCLASSIFIED.)

6. Flow reversal caused by cavity pressures in excess of that in the rocket chamber .

7. Deformation of the crack geometry due to burning and pressure loading .

8. Propagation of the crack tip due to regression and mechanical fracture.

In addition to these interrelated phenomena, there are many other important factors which can influence the crack combustion process. These factors include:

1. Initial geometry of the crack

2. Variation of rocket chamber conditions

3. Erosive burning effects due to high gas velocities

4. Dynamic burning effects due to rapid pressure transients

5. Physiochemical properties of the propellant

6. Initial temperature of the propellant.

Although imperfections in solid propellant grains may be distributed in an irregular intricate network, a rational starting-point for understanding the complicated interaction of the above-mentioned phenomena is to consider a simple ordered system--a single isolated crack. For such a system, it is desirable to establish a criterion for stable combustion without catastrophic crack propagation; the delineation of a safe domain of governing parameters is the ultimate goal. But before it can be achieved, a realistic theoretical model describing the transient combustion processes inside a propellant crack has to be established and experimentally verified.

The current research program was undertaken to experimentally and theoretically investigate the complex problem of transient combustion within a propellant crack. The objectives of the work for this reporting period are:

1. To establish a theoretical model for predicting the rate of flame propagation inside a single isolated crack of variable geometry.

4

2. To predict the pressure distribution and pressurization rate inside a crack, leading to a basis for calculating overall stress loading in the crack.

3. To parametrically investigate the influence of crack geometry, main chamber pressurization rate, and other physiochemical parameters on the gasification rate inside the propellant cavity.

4. To design and test an experimental combustion chamber for verification of the theoretical model and for establishment of a fundamental data base in crack combustion.

This report has been written to document the progress gained toward achieving a better understanding of transient crack combustion. The Background section reviews some of the previous analytical and experimental studies in crack combustion, and "Theoretical Modeling" describes the boundary conditions and numerical solution procedures. In "Experimental Apparatus and Procedure," the experimental combustion chamber and data acquisition system are discussed. "Discussion of Results" describes the theoretical results of a parameter study along with a comparison of theory with limited experimental data. Finally, the progress achieved and the conclusions drawn from the results obtained are summarized in the "Summary of Progress and Conclusions."

BACKGROUND

Although the overall process of transient crack combustion is extremely complicated, various investigations have been conducted to study certain particular processes described earlier.

Taylor conducted experimental tests to study the convective burning of porous propellants with closed- and open-end boundary conditions.[2] He observed a critical pressure above which the hot gas can penetrate into the porous propellant and significantly increase the regression rate of the charge. His experiments revealed that the flame front decelerated in a region near the closed end of the propellant charge.

---

[2]J. W. Taylor. "The Burning of Secondary Explosive Powders by a Convective Mechanism," *Trans Farad, Soc*, Vol. 58, 1962, p. 561.

Prentice studied the flame spreading phenomena in transient solid propellant cracks using high speed motion pictures and fine thermocouples.[3] Difficulties were encountered in using fine thermocouples due to the long response time of the thermocouple, uncertainty in the precise location of the thermocouple, and also due to the gaseous explosion. For closed-end cracks, with small diameters, he observed that the flame cannot propagate into the crack when the bomb pressure is low.

Bobolev, et al., studied the mechanism by which combustion products penetrate into the propellant crack.[4] Two mechanisms were proposed: (1) forced penetration of gas due to a higher external pressure, followed by (2) "spontaneous penetration" of product gases from the crack surface into the unburned region of the propellant crack.

Belyaev, et al, showed that burning of propellant inside a narrow pore may lead to an excess pressure build-up.[5] Their experimental results have indicated that the erosive burning effect cannot be neglected in the crack combustion study.

In a later study, Belyaev, et al., made a series of experimental tests to study the dependence of flame spreading rate on crack geometry, propellant properties, boundary conditions, and combustion chamber pressures.[6] Part of their experiments were conducted in the atmosphere and in a "constant pressure" Crawford vessel where the initial pressure in the crack was equal to the bulk pressure in the vessel. They found that both the flame-spreading rate and pressure gradient along a crack are strong functions of crack width. For a closed-end crack, they observed that the flame-spreading rate increases initially until reaching a constant speed and then decelerates near the tip of the crack.

---

[3]Naval Ordnance Test Station. *Flashdown in Solid Propellants*, by J. L. Prentice. China Lake, Calif., NOTS, December 1962. (NOTS TP 3009, publication UNCLASSIFIED.)

[4]V. K. Bobolev, A. D. Margolin, and S. V. Chuiko. "The Mechanism by Which Combustion Products Penetrate into the Pores of a Charge of Explosive Material," *Doklady Akademii Nauk*, USSR, Vol. 162, No. 2, May 1965, pp. 388-391.

[5]A. F. Belyaev, et al. "Development of Combustion in an Isolated Pore," *Combustion, Explosion & Shock Waves*, Vol. 5, No. 1, Jan-Mar 1969, pp. 4-9.

[6]A. F. Belyaev, et al. "Development of Burning in a Single Pore," *Transition of Combustion of Condensed Systems to Detonation*, Chapter 5, Part A, Section 22, Science Publisher, 1973, pp. 115-134.

Cherepanov stated that in a sufficiently narrow and long cavity, as a result of the impeded gas flow, the pressure reaches such high values that the system becomes unstable.[7] He further divided the instability mechanism into two different physical forms: (1) local volume burning at the end of the cavity, and (2) local destruction of the propellant. In his theoretical analysis, steady-state conditions were assumed, but this is not practical in a real case. The ignition criterion was not established in the analysis, and the continuity equation did not include the mass addition due to burning. Friction loss in the momentum equation was also neglected. Energy release due to combustion and energy loss from the hot gas to the unburned propellant was ignored. Thus, the analysis cannot predict the flame propagation and the actual combustion phenomena inside a propellant crack.

Margolin, et al., indicated that the spontaneous penetration of combustion gases into the pores of a gas-permeable explosive charge occurs when the Andreev number (An) is beyond its critical value.[8] The boundary conditions were found to be important in flame propagation. Godai, in his experiment, indicated that a threshold diameter or a critical width of a uniform cavity exists, below which flame will not propagate into the crack.[9].

Krasnov, et al., investigated the rate of penetration of combustion into the pores of an explosive charge.[10] The experiment was performed in a constant-pressure bomb. The experimental results showed that the flame spreading rate is not equal to the rate of penetration of the combustion products into the channel. Their theoretical model was based on the following crude assumptions: (1) constant thermal wave penetration depth in the heated propellant along the flow direction,

[7]G. P. Cherepanov. "Combustion in Narrow Cavities," *J APPL MECH & TECH PHY*, Vol. 11, No. 2, 1970, pp. 276-281.

[8]A. D. Margolin and V. M. Margulis. "Penetration of Combustion into an Isolated Pore in an Explosive," *Combustion, Explosion & Shock Waves*, Vol. 5, No. 1, 1969, pp. 15-16.

[9]T. Godai. "Flame Propagation into the Crack of a Solid-Propellant Grain," *AMER INST AERONAUT & ASTRONAUT J*, Vol. 8, No. 7, July 1970, pp. 1322-1327.

[10]Yu. K. Krasnov, et al. "Rate of Penetration of Combustion into the Pores of an Explosive Charge," *Combustion, Explosion & Shock Waves*, Vol. 6, No. 3, 1970, pp. 262-265.

(2) uniform temperature profile inside the heated propellant layer, and
(3) steady-state assumptions for the heat balance equation. Hence,
their theoretical approach is inadequate for predicting flame spreading.

Jacobs, et al., studied the pressure distributions in burning
cracks which simulate the separation or debond of solid propellants from
the motor casing.[11] Wedge-shaped channels with debond angles of 4.75,
3.17, and 1.90 degrees were tested in a combustion chamber at various
levels of pre-pressurization. Pressure measurements were obtained at
three locations along the debond and at one location in the pressure
chamber. The propellant was doped with a highly flammable mixture of
titanium and ammonium perchlorate powder so that ignition under in-
creased pressures could be safely assumed to approach that of instan-
taneous ignition over the entire surface. This ignition procedure was
perhaps advantageous for them to compare the experimental results with a
quasi-steady theoretical model. The actual ignition and flame spreading
processes were avoided. Therefore, their analytical results cannot be
used to predict any transient behavior in crack combustion.

Other studies of combustion inside propellant cracks can be found
in the literature.[12-14] Although many interesting experimental results
have been obtained, no sound theoretical model was developed to describe
the transient processes governing crack combustion.

[11]Air Force Rocket Propulsion Laboratory. *An Experimental Study of*
the Pressure Distribution in Burning Flaws in Solid Propellant Grains,
by H. R. Jacobs, et al., University of Utah. Edwards, Calif., AFRPL,
October 1972. (AFRPL-TR-72-108, publication UNCLASSIFIED.)

[12]A. F. Belyaev, et al. "Consequences of the Penetration of Combus-
tion into an Individual Pore," *Combustion, Explosion & Shock Waves,* Vol.
6, No. 2, April-June 1970, pp. 149-153.

[13]E. C. Francis, G. H. Lindsey, and R. R. Parmerter. "Pressurized
Crack Behavior in Two-Dimensional Rocket Motor Geometries," *AMER INST*
AERONAUT ASTRONAUT J, Vol. 9, No. 6, June 1972, pp. 415-419.

[14]Z. V. Kirsanova and O. I. Leipunskii. "Investigation of the
Mechanical Stability of Burning Cracks in a Propellant," *Combustion,*
Explosion & Shock Waves, Vol. 6, No. 1, 1970, pp. 68-75.

THEORETICAL MODELING

The physical model chosen to simulate a crack in a propellant grain is depicted schematically in Figure 1. It represents a pore located in the transverse direction to the main flow of the rocket chamber. The crack can be of variable geometry with the opening initially starting at or near the propellant surface which is exposed to the main chamber flow. This physical model can also be easily extended to simulate conditions of debond or separation of the propellant from the motor casing.
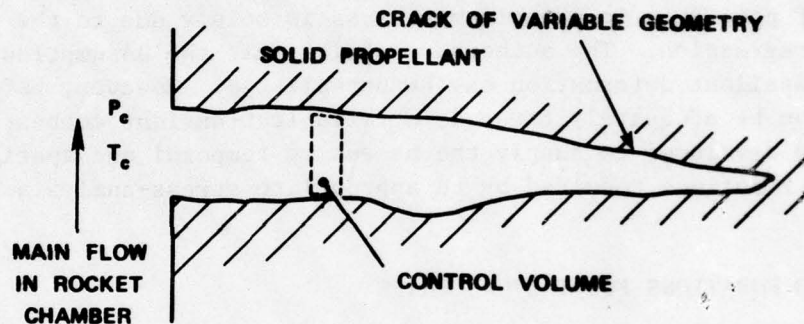
FIGURE 1. The Physical Model of a Transverse Crack in Solid Propellant.

The following basic assumptions are used to facilitate a theoretical description of the transient combustion processes inside a crack:

1. All chemical reactions occur near the propellant crack surface, in a combustion zone which is so thin that it can be considered as a plane. That is, the thickness of the combustion zone above the propellant surface is much smaller than the gap width in the propellant crack.

9

2. Rate processes at the propellant surface are quasi-steady in the sense that the characteristic times associated with the gaseous flame and preheated propellant are short compared to that of the pressure transient variation.

3. The gases flowing in the propellant crack obey the Clausius or Noble-Abel equation of state. This dense gas relation can adequately describe the departure from the ideal gas law at high pressures.

4. The bulk flow in the pore is one-dimensional. Recent experiments[15] conducted by Kuo, et al., have revealed that the one-dimensional assumption is appropriate for flow in cracks when the pressure gradient along the crack is greater than a critical value which normally is extremely small.

5. The compressibility of the solid propellant is neglected. The change of port area in propellant cracks is solely due to the propellant surface regression. The authors recognize that the assumption of negligible propellant deformation may be unrealistic. However, before this effect can be adequately treated, a reliable transient combustion model has to be developed to supply the necessary temporal and spatial pressure distributions required by an appropriate stress-analysis code.

GOVERNING EQUATIONS FOR THE GAS PHASE

To describe the transient gas-phase behavior inside a propellant crack, we derive the unsteady, quasi-one-dimensional mass, momentum and energy equations from a balance of fluxes which act on an elemental control volume as shown in Figure 1. The resultant conservation equations expressed in divergence form are:

Mass Conservation

$$\frac{\partial(\rho A_p)}{\partial} + \frac{\partial(\rho u A_p)}{\partial} = r_b \, \rho_{pr} \, \mathscr{P}_b \tag{1}$$

---

[15]K. K. Kuo, A. T. Chen, and T. R. Davis. "Transient Flame Spreading and Combustion Processes inside a Solid Propellant Crack," presented at *15th AIAA Aerospace Sciences Meeting*, January 1977. (AIAA Paper No. 77-14)

10

Momentum Conservation

$$\frac{\partial}{\partial t} (\rho \, u \, A_p) + \frac{\partial}{\partial x} (\rho \, A_p \, u^2) = -g \, A_p \, \frac{\partial P}{\partial x}$$

$$+ \, g \, \frac{\partial}{\partial x} (A_p \, \tau_{xx}) - \mathscr{P}_w \, \tau_w \, g \, \cos\theta_w$$

$$+ \, \rho \, A_p \, B_x \, g - (\rho_{pr} \, r_b \, \mathscr{P}_b) \, V_{gf} \, \sin\theta_w \qquad (2)$$

Energy Conservation

$$\frac{\partial}{\partial t} (\rho \, A_p \, E) + \frac{\partial}{\partial x} (\rho \, A_p \, u \, E) = \frac{\partial}{\partial x} \left(\lambda \, A_p \, \frac{\partial T}{\partial x} \right)$$

$$- \, \frac{1}{J} \, \frac{\partial}{\partial x} (A_p \, P \, u) + \frac{1}{J} \, \frac{\partial}{\partial x} (\tau_{xx} \, A_p \, u)$$

$$+ \, \rho_{pr} \, r_b \, \mathscr{P}_b \, h_f - \bar{h}_{cp} \, \mathscr{P}_b \, (T - T_{ps})$$

$$+ \, \frac{B_x \, \rho \, A_p \, u}{J} - \bar{h}_{cw} \, (\mathscr{P}_w - \mathscr{P}_b)(T - T_{ws}) \qquad (3)$$

The conservation equations are simplified further by an order-of-magnitude analysis which shows that the following terms are negligible:

1. Forces between gas molecules due to the viscous normal stress in the axial direction, created by the axial velocity gradient in the momentum equation

2. Viscous dissipation and rate of work done by the force due to viscous normal stresses in the energy equation

3. Axial heat conduction between gas molecules in the energy equation.

After rearranging the conservation equations, a set of three governing equations is obtained, i.e., velocity-variation, temperature-variation, and pressure-variation equations which are shown below.

11

Velocity-Variation Equation

$$\frac{\partial u}{\partial t} + u \frac{\partial u}{\partial x} + \frac{g}{\rho} \frac{\partial P}{\partial x} = -\mathscr{P}_w c_f \frac{u|u|\cos\theta_w}{2A_p} - \frac{r_b \mathscr{P}_b r \rho_{pr}}{A_p \rho}$$

$$- \frac{\rho_{pr} r_b \mathscr{P}_b v_{gf} \sin\theta_w}{A_p \rho} + B_x g \qquad (4)$$

Temperature-Variation Equation

$$\frac{\partial T}{\partial t} + u \frac{\partial T}{\partial x} + \frac{P(\gamma-1)}{\rho R} \frac{\partial u}{\partial x} = - \frac{Pu(\gamma-1)}{A_p \rho R} A_{px}$$

$$+ \frac{\gamma \rho_{pr} r_b \mathscr{P}_b}{A_p \rho} \left(T_f - \frac{T}{\gamma} + \frac{u^2}{2g J c_p}\right)$$

$$- \frac{\bar{h}_{cp} \mathscr{P}_b J}{\rho A_p R} (T-T_{ps})(\gamma-1) - (\gamma-1) J \frac{\bar{h}_{cw}}{\rho A_p} \frac{(\mathscr{P}_w - \mathscr{P}_b)}{R} (T-T_{ws})$$

$$+ (\gamma-1) \frac{\mathscr{P}_w c_f u^2 |u|\cos\theta_w}{2g A_p R} + (\gamma-1) \frac{\rho_{pr} r_b \mathscr{P}_b u v_{gf} \sin\theta_w}{\rho g R A_p} \qquad (5)$$

Pressure-Variation Equation

$$\frac{\partial P}{\partial t} + u \frac{\partial P}{\partial x} + \frac{\gamma P^2}{\rho R T} \frac{\partial u}{\partial x} = \frac{r_b \mathscr{P}_b P^2}{\rho^2 A_p R T} (\rho_{pr} - \rho) - \frac{\gamma P^2 u}{A_p \rho R T} A_{px}$$

$$+ \frac{\gamma \rho_{pr} r_b \mathscr{P}_b P}{A_p \rho T} \left(T_f - \frac{T}{\gamma} + \frac{u^2}{2g J c_p}\right) - (\gamma-1) \frac{\bar{h}_{cp} \mathscr{P}_b J P}{A_p \rho R T} (T-T_{ps})$$

$$- (\gamma-1) \frac{\bar{h}_{cw} J P}{\rho A_p R T} (\mathscr{P}_w - \mathscr{P}_b)(T-T_{ws}) + (\gamma-1) \frac{\mathscr{P}_w c_f P U^2 |u|\cos\theta_w}{2g A_p R T}$$

$$+ (\gamma-1) \frac{\rho_{pr} r_b \mathscr{P}_b P u v_{gf} \sin\theta_w}{A_p g \rho R T} \qquad (6)$$

The three governing equations are first order, coupled, inhomogeneous, and non-linear partial differential equations. The unknowns which vary strongly with respect to the spatial variables are: gas temperature, pressure, velocity and the temperatures at the propellant surface and inert wall if present. There are other unknown parameters which vary weakly with respect to spatial variables. These parameters include the port area of the crack, the burning rate of the propellant, the convective heat transfer and friction coefficients, the gas flow angle, the local blowing velocity normal to the propellant surface, the wetted perimeter and the burning perimeter at various locations along the crack.

In order to solve all the unknowns mentioned above, additional equations and boundary conditions together with some physical input functions must be specified. The equation which governs the surface temperature variation of the solid phase is described below.

EQUATION FOR DETERMINATION OF PROPELLANT SURFACE TEMPERATURE

The propellant surface temperature at a fixed location along the crack before the attainment of ignition is calculated from the solid-phase heat conduction equation which is written in the unsteady, one-dimensional form

$$\frac{\partial T_{pr}(t, y)}{\partial t} = \alpha_{pr} \frac{\partial^2 T_{pr}(t, y)}{\partial y^2} \tag{7}$$

where the length variable, y, is measured perpendicular to the local propellant crack surface.

Since this equation is first order in time derivative and second order in space derivative, the following initial and boundary conditions are required

$$T_{pr}(0, y) = T_{pi} \tag{8}$$

$$T_{pr}(t, \infty) = T_{pi} \tag{9}$$

$$\frac{\partial T_{pr}}{\partial y}(t, 0) = -\frac{\bar{h}_c(t)}{\lambda_{pr}}[T(t) - T_{ps}(t)] \tag{10}$$

13

An approximate solution of the heat equation, which is quite accurate and saves much computation time may be obtained by using the integral method.[16,17] Applying this method, a quantity $\delta_t(t)$ (called the thermal penetration distance) is defined, so that the $y \geq \delta_t$, the solid is at equilibrium temperature, and there is no heat transfer. It is illustrated in Figure 2.
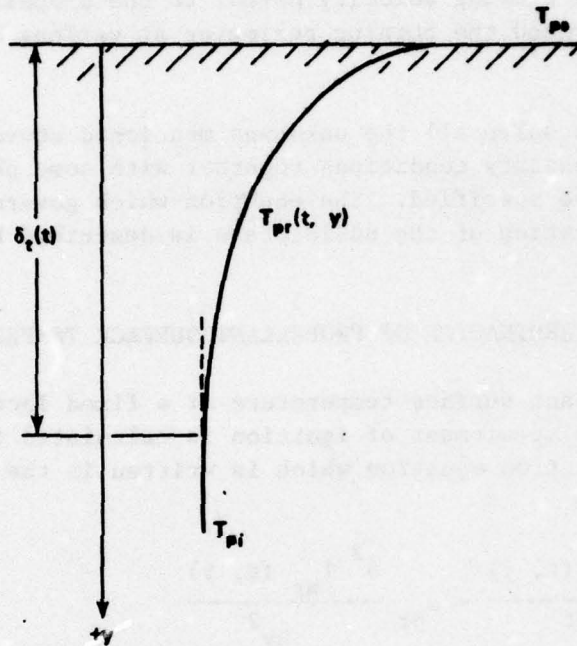
FIGURE 2. Temperature Profile in the Solid Propellant.

A third degree polynomial is used with time varying coefficients to approximate the transient temperature profile in the solid phase

$$T_{pr} = k_0(t) + k_1(t) \, y + k_2(t) \, y^2 + k_3(t) \, y^3 \qquad (11)$$

---

[16]T. R. Goodman. "The Heating of Slabs with Arbitrary Heat Inputs," *J AEROSPACE SCI*, Vol. 26, March 1959, pp. 183-188.

[17]T. R. Goodman. "Application of Integral Methods to Transient Non-linear Heat Transfer," *Advances in Heat Transfer*, Vol. 1, 1964, Academic Press, New York, pp. 51-122.

14

where the coefficients k_0, k_1, k_2, and k_3 may be time-dependent. To determine them, four boundary conditions are necessary. These are

$$T_{pr}(t, \delta_t) = T_{pi} \tag{12}$$

$$\frac{\partial T_{pr}}{\partial y}(t, \delta_t) = 0 \tag{13}$$

$$\frac{\partial^2 T_{pr}}{\partial y^2}(t, \delta_t) = 0 \tag{14}$$

$$\frac{\partial T_{pr}}{\partial y}(t, 0) = -\frac{\bar{h}_c}{\lambda_{pr}}[T(t) - T_{ps}(t)] \tag{15}$$

After applying the integral method, the resulting ordinary differential equation describing the rate of increase of propellant surface temperature is

$$\frac{d T_{ps}}{dt} = \frac{4 \alpha_{pr} \bar{h}_c^2 (T - T_{ps})^3}{3\lambda_{pr}^2 (T_{ps} - T_{pi})(2T - T_{ps} - T_{pi})} \tag{16}$$

The initial condition used for this equation is: $T_{ps} = T_{pi} + \epsilon$, where ϵ is a small value used to avoid singularity.

EQUATION OF STATE FOR GAS AND SOLID PHASES

In addition to the governing equations in the gas phase and the equation describing the rate of increase in T_{ps}, the equation of state for the gas and solid phases must be specified. As discussed earlier, the Clausius or Noble-Abel equation of state

$$P(1/\rho - b) = RT \tag{17}$$

was chosen to account for any non-ideal gas behavior. The term, b, represents the co-volume or volume occupied by the individual gas molecules. One obvious advantage of using the Noble-Abel equation of state is its flexibility; it can be readily reduced to the ideal gas equation

15

by setting the value of the co-volume to zero. The statement of constant density for the solid propellant serves as the equation of state for the solid phase.

EMPIRICAL HEAT TRANSFER AND FRICTION COEFFICIENT CORRELATION

The expression for the local convective heat-transfer coefficient, $\bar{h}_c$, is deduced from the conventional Dittus-Boelter correlation for turbulent flow in pipes.[18] Variation of the physical properties of the gas across the boundary layer is considered by evaluating the properties at an average film temperature, T_{af}. The expression for h_c, used in the model, is

$$\bar{h}_c = 0.0346 \, Pr^{-0.6} \, c_p (P \, u/R)^{0.8} \, V_k^{0.2} \, T_{af}^{-0.67} \, (x \, d_h)^{-0.1} \quad (18)$$

Before local ignition $\bar{h}_{cp} = \bar{h}_{cw} = \bar{h}_c$, whereas after local ignition $h_{cp} = 0$ and $h_{cw} = h_c$.

The above equation has incorporated the temperature dependence of the viscosity which was determined from the calculations of Svehla for the viscosity of air at high temperature.[19] It was shown by Bartz that Svehla's values are very close to those in the previously published NBS data.[20,21] The coefficient of viscosity-temperature relation, V_k, is defined as

$$V_k = 8.699 \times 10^{-7} \, M_w^{0.5} \quad (19)$$

---

[18]A. Peretz, et al. "Starting Transient of Solid Propellant Rocket Motors with High Internal Gas Velocities," *AMER INST AERONAUT ASTRONAUT J*, Vol. 11, No. 12, December 1973, pp. 1719-1727.

[19]National Aeronautics and Space Administration. *Estimated Viscosities and Thermal Conductivities of Gases at High Temperatures*, by R. A. Svehla. Cleveland, Ohio, NASA, 1962. (Publication UNCLASSIFIED.)

[20]D. R. Bartz. "Survey of the Relationship Between Theory and Experiment for Convective Heat Transfer from Rocket Combustion Gases," *Advances in Tactical Rocket Propulsion, AGARD Conference Proceedings No. 1.* Technivision Services, Maidenhead, England, August 1968, pp. 291-381.

[21]J. Hilsenrath, et al. *Tables of Thermal Properties of Gases*, U.S. Department of Commerce, NBS Circular 564, November 1955.

The Prandtl number is calculated from Svehla's equation[19]

$$Pr = \frac{\gamma}{1.77\,\gamma - 0.45} \tag{20}$$

The correlation for the friction coefficient used in this study is

$$c_f = \frac{0.4491\,(d_h/x)^{0.1}}{\left\{\ln\left[\dfrac{\varepsilon_s/d_h}{3.7} + \dfrac{1.46\,RV_k T_{af}^{1.65}\,(d_h/x)^{0.05}}{p\,u\,d_h\,c_f^{0.5}}\right]\right\}^2} \tag{21}$$

where ε_s/d_h is the relative equivalent sand roughness. This expression is actually a modified form of the well-known Colebrook formula[22,23] for turbulent flow in pipes with roughness. Entrance effects are taken into account by modifying the friction coefficient by a power function of the distance-to-diameter ratio; the original Colebrook expression is obtained for $s/d_h \geq 20$. Additionally, Eq. (21) implicitly accounts for the temperature dependence of the gas density and viscosity, each evaluated at the average film temperature, T_{af}.

After the propellant surface starts burning locally, the value of the friction coefficient is set to zero due to the attenuation of wall shear stress caused by surface blowing.

PROPELLANT BURNING RATE EXPRESSION

In the absence of a more adequate erosive burning rate expression, the Lenoir-Robillard burning rate formula[24] is used temporarily to account for the erosive burning effect

$$r_b = a\,P^n + K_e \bar{h}_c \exp(-\beta\,r_b\,\rho_{pr}/u\,\rho) \tag{22}$$

[22]H. Schlicting. "Turbulent Flow Through Pipes," *Boundary Layer Theory*, 6th Ed., McGraw-Hill, New York, 1968.

[23]C. F. Colebrook. "Turbulent Flow in Pipes with Particular Reference to the Transition Region Between the Smooth and Rough Pipe Laws," *J Inst Civil Engineers*, Vol. 11, pp. 133-156, 1938-39.

[24]J. M. Lenoir and G. Robillard. "A Mathematical Method to Predict the Effects of Erosive Burning in Solid Propellant Rockets," *6th Symp. (Int.) on Combustion*, The Combustion Institute (1956), pp. 663-7.

This relation is actually a modified form of the Lenoir-Robillard formula, since the original expression proposed for $\bar{h}_c$ is based on the Chilton-Colburn correlation for turbulent flow over a flat plate, whereas the expression for h_c in Eq. (22) is the modified Dittus-Boelter correlation (Eq. (18)). The local burning rate as given by the above relation is strongly coupled to the gas dynamics inside the crack.

PROPELLANT IGNITION CRITERION

After T_{ps} is solved, a simplified ignition temperature criterion is used to determine the burning condition of the solid propellant along the crack. In order to avoid the step function change in burning rate, a two-temperature criterion is used to achieve full ignition within a finite time interval; when T_{ps} is equal to T_{cri}, the propellant starts to gasify. As soon as T_{ps} reaches T_{ign}, the full ignition condition is reached.

INITIAL AND BOUNDARY CONDITIONS

The initial conditions required for the solution of the system of governing equations are:

$$u(0, x) = u_i$$
$$T(0, x) = T_i$$
$$P(0, x) = P_i \tag{23}$$

where u_i, T_i, and P_i are the initial velocity, temperature, and pressure in the propellant crack.

The number of boundary conditions required depends upon the flow direction and Mach number at the opening of the crack. When the gas in the rocket chamber flows subsonically into the propellant crack, two boundary conditions at the opening of the propellant crack are specified to represent the interface conditions at the crack entrance; and one boundary condition at the closed end of the propellant crack is specified to indicate that the gas velocity is zero. In the mathematical form they are represented as follows:

$$P(t, 0) = P_c(t)$$
$$T(t, 0) = T_c(t)$$
$$u(t, x_L) = 0 \tag{24}$$

18

When the flow of the gas out of the crack is subsonic, two boundary conditions are specified. They are written as

$$P(t, 0) = P_c(t)$$
$$u(t, x_L) = 0 \qquad (25)$$

When the outflowing gas is supersonic, only one boundary condition can be specified, that is

$$u(t, x_L) = 0 \qquad (26)$$

In order to solve the system of governing equations with a second order numerical scheme, extraneous boundary conditions are required in addition to the physical ones. The procedure to attain these conditions is discussed in the following section.

NUMERICAL SOLUTION TECHNIQUE

The governing equations (Eq. (4) through (6)), describing the dynamic behavior of a Noble-Abel dense gas in a propellant crack were found to be totally hyperbolic.[25] The numerical techniques developed were chosen on the basis of stability, maximum accuracy, and computational efficiency. Recently obtained experience in solving hyperbolic partial differential equations[26] was utilized, and a generalized implicit scheme[27,28] based on central differences in space-wise derivatives was chosen to solve the governing equations. A quasi-linearization method, used to linearize the inhomogeneous terms in the governing equation, was combined with a stable predictor-corrector procedure.[29] Finally, the governing equations, in their finite-difference form, were arranged in a block-tridiagonal matrix form,[29] which allowed an efficient computation.

---

[25]R. Courant and D. Hilbert. *Methods of Mathematical Physics*, Vol. 2, Interscience Publishers, Inc., New York, July 1966, pp. 407-550.

[26]K. K. Kuo. "Theory of Flame Front Propagation in Porous Propellant Charges under Confinement," Ph.D. Thesis. Princeton University, Princeton, N. J., August 1971. (AMS Report T-1000.)

[27]R. D. Richtmyer and D. W. Morton. *Difference Methods for Initial-Value Problems*. Interscience Publishers, New York, 1967.

[28]M. G. Salvadori and M. L. Baron. *Numerical Methods in Engineering*. Englewood Cliffs, N. J., Prentice Hall, 1961.

[29]A. T. Chen. "Theoretical Modeling and Numerical Solution of Transient Flame-Spreading in Solid-Propellant Cracks," M.S. Thesis, Mechanical Engineering Department, Pennsylvania State University, May 1976.

The use of central difference formulation for all spacewise derivatives in the governing equations requires six boundary conditions for the solution. This implies that when the gas flows into the crack, three extraneous boundary conditions are required in addition to the three physical ones described by Eq. (24). The three extraneous boundary conditions are used to determine the flow velocity at the opening of the crack, and the pressure and temperature at the closed end of the crack.

When the gas flows out of the crack subsonically, in addition to the two physical boundary conditions described by Eq. (25), two extraneous boundary conditions are required at the opening of the crack for the determination of the pressure and temperature. Also, two extraneous boundary conditions are required at the closed end of the crack.

When the outflowing gas is supersonic, in addition to the physical boundary condition given by Eq. (26), three extraneous boundary conditions are needed at the opening of the crack and two other extraneous boundary conditions are needed at the tip of the crack.

These extraneous boundary conditions, which are also frequently called compatibility relations, are given below:

$$\left[\frac{dP}{dt}\right]_{I,II} = \pm \frac{\gamma P^2}{\rho RT} \frac{1}{C} \left[\frac{du}{dt}\right]_{I,II} + \left[F_p \pm F_u \frac{\gamma P^2}{\rho RT_c}\right]_{I,II} \tag{27}$$

$$\left[\frac{dT}{dt}\right]_{III} = \frac{T(\gamma - 1)}{\gamma P} \left[\frac{dP}{dt}\right]_{III} + \left[F_T - F_p \frac{T(\gamma - 1)}{\gamma P}\right]_{III} \tag{28}$$

where F_u, F_T, and F_p represent the inhomogeneous terms on the right hand side of Eq. (4), (5), and (6). The subscripts I, II, and III designate the right-running, left-running characteristic lines and the particle path line, respectively. These relations were obtained by transforming the governing hyperbolic equations into their characteristic form. Together with the physical boundary conditions, the compatibility relations form a closed system for the determination of velocity, temperature, and pressure at both ends of the crack.

The extraneous boundary conditions are numerically evaluated by a fourth order Runge-Kutta integration technique. In previous calculations, the integration of each compatibility relation was treated consecutively. Currently, these equations are simultaneously integrated to improve the numerical stability of the solution.

EXPERIMENTAL APPARATUS AND PROCEDURE

TEST RIG DESIGN

An overall view of the experimental combustion chamber used to study the flame spreading and pressurization phenomena in propellant cracks is shown in Figure 3. The design of this test rig was guided by the following primary considerations:
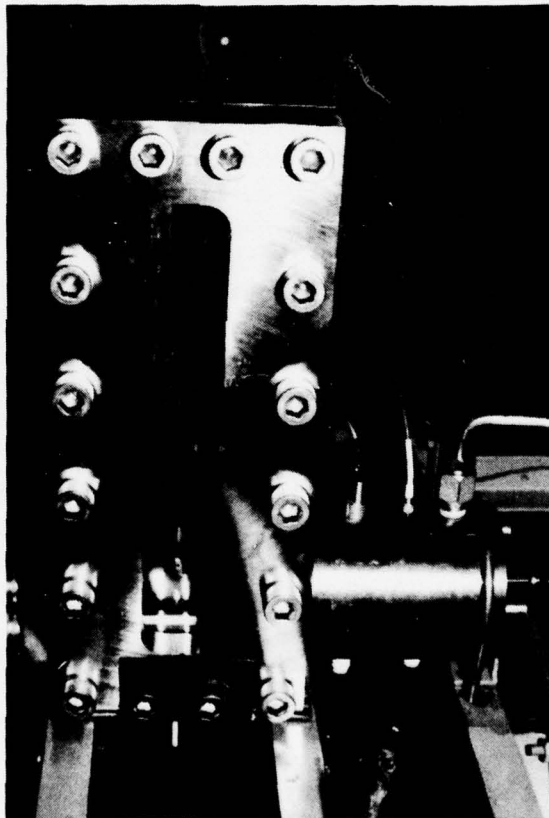
FIGURE 3. Overall View of the Assembled Gaseous Ignition System Mounted With the Combustion Chamber on the Test Stand.

1. The experimental set-up should be as close as possible to the physical conditions considered in the analytical model so that the experimental results can be used directly for the verification of the theoretical solutions.

2. The test rig should have sufficient flexibility to permit a wide range of variation in propellant crack geometry, properties, chamber pressure, pressurization rate, igniter gas temperature and the main chamber mass flow rate in the transverse direction to the crack. This flexibility in testing is essential for the establishment of a fundamental data base in propellant crack combustion.

A schematic diagram of the test rig is shown in Figure 4, and an assembly view of the propellant crack combustion chamber is shown in Figure 5. The propellant containing a simulated crack is cast into a brass mold. A special mandrel is used during the propellant molding process to produce a 2.54 cm deep, channel-shaped crack of length, L, and gap width, δ. Thus far, two different crack geometries have been used: for the large crack, $L = 20$ cm and the average, $\delta = 0.52$ cm; for the small crack, $L = 15$ cm and the average, $\delta = 0.08$ cm. The main block of the combustion chamber has five parts machined into its backside along the longitudinal axis of the crack to accept four piezoelectric pressure transducers and a safety burst diaphragm. The pressure transducers are located at a distance of 0.0, 4.8, 13.8, and 18.8 cm from the initial crack opening. The window assembly consists of a 1/4-inch sacrificial Plexiglas plate and a main Plexiglas window. This window assembly along with a stainless steel retainer is used to close the combustion chamber and permit visual recording of the luminous flame front inside the propellant crack. An interchangeable exit nozzle is connected to the combustion chamber for control of the rate of chamber pressurization. The combustion chamber was designed for a maximum static pressure of 800 atmospheres.

An ignition system has been developed using spark plugs to ignite a gaseous mixture of oxygen and methane. A schematic drawing of the igniter system is shown in Figure 6. Both fuel and oxidizer feedlines contain a pressure regulator and critical flow orifice which permit exact control of the fuel-oxidizer flow rates. The gaseous reactants are first mixed in the igniter chamber by tangentially injecting methane into the oxygen flow stream. The mixed reactants then enter the test section through a rectangularly oriented, multi-perforated, convergent nozzle. This versatile igniter design provides the necessary variability to produce a wide range of igniter strength.
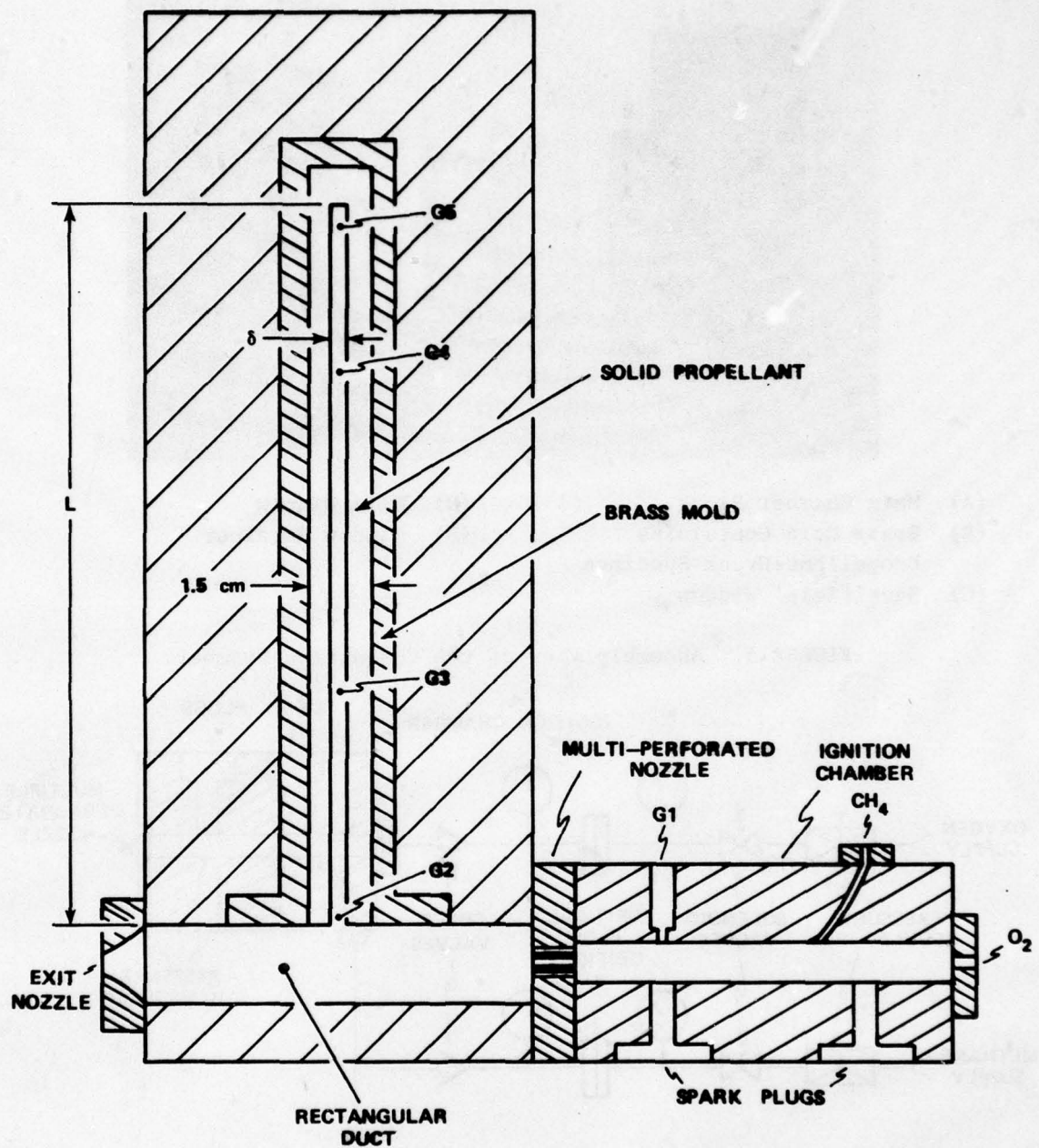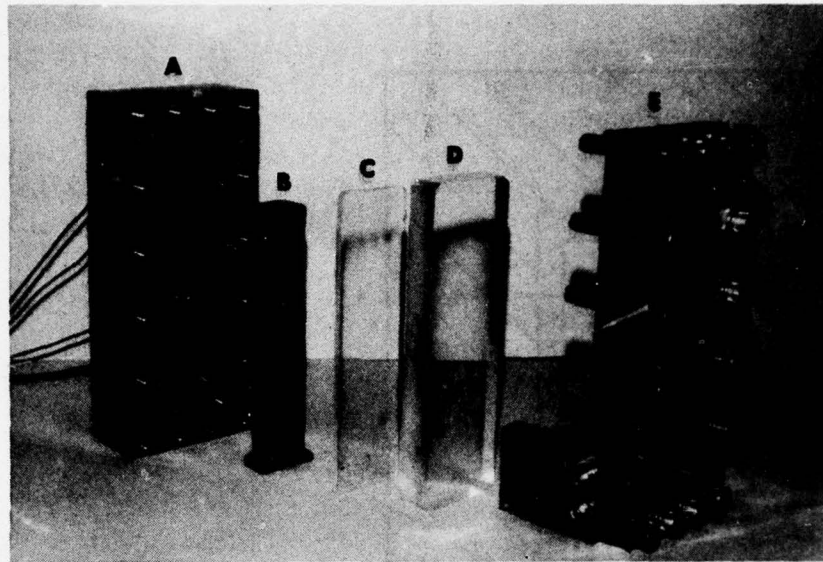
22

FIGURE 4. Schematic Diagram of Propellant Crack Combustor.

23

(A) Main Chamber Block
(B) Brass Mold Containing
    Propellant-Crack Specimen
(C) Sacrificial Window
(D) Main Window
(E) Window Retainer

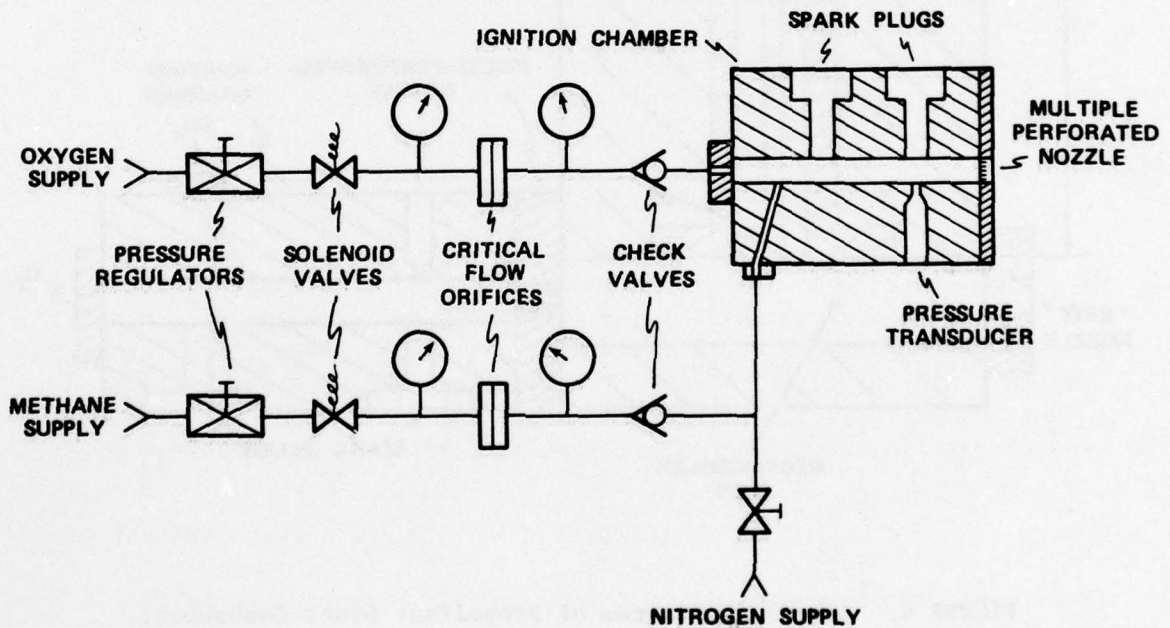FIGURE 5. Assembly View of the Combustion Chamber.

FIGURE 6. Schematic Diagram of the Gaseous Ignition System.

24

INSTRUMENTATION

A block diagram of the data acquisition system is shown in Figure 7. The components of this instrumentation system are:

1. A high-speed magnetic tape recorder (Hewlett Packard model 3924B) with a simultaneous 14 channel record/reproduce capability at a rate up to 60 in/s. Seven channels record in FM mode, and the other seven channels record in the direct or AM mode.

2. An analog-to-digital converter (Biomation 1015 Transient Waveform Digitizer) provides 4-channel data storage with 1024 word memory per channel, and is capable of a real-time resolution down to 10 μs. The output of the analog-to-digital converter is used to control the horizontal and vertical deflection of an X-Y plotter to obtain a hard copy of the transient data.

3. A 16 mm high-speed camera (FASTAX Model W-163269) is used with a 100-foot film roll to record the propagation of the luminous flame front and regression of the propellant surface.
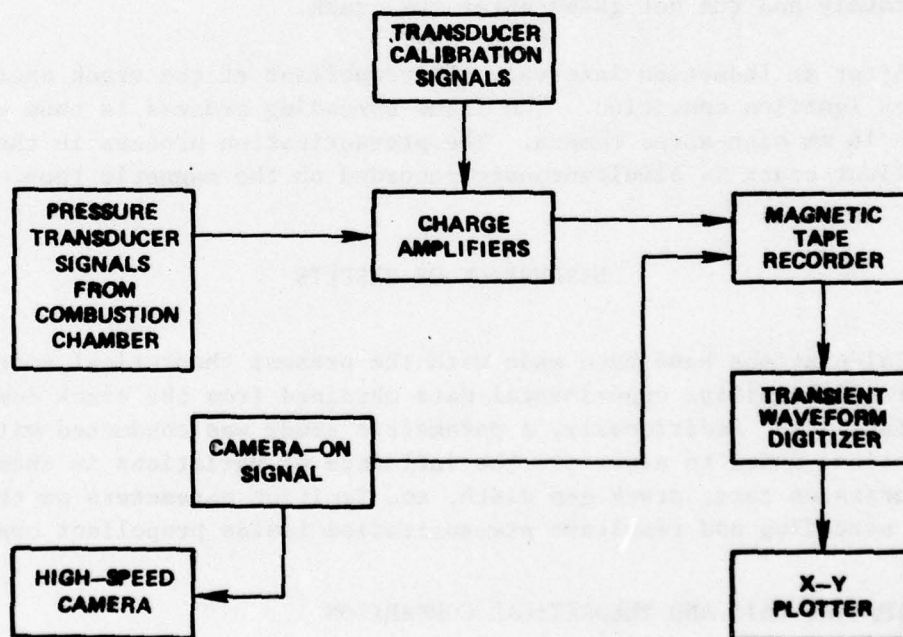

FIGURE 7. Block Diagram of the Instrumentation System.

25

4.   Piezoelectric pressure transducers (Kistler Model 601B)
equipped with water-cooled adapters (Kistler Model 628C) are used to
measure the pressure at four locations along the propellant crack.
Charge amplifiers (Kistler Model 504 E Dual Mode Amplifiers) are used to
condition the pressure signal for tape recording. These transducers are
recess-mounted in the combustion chamber and can be used to measure
pressures up to 1000 atmospheres.

TEST PROCEDURE

A typical test firing is conducted in the following manner. In
order to prevent unburned igniter gases from entering the crack, a strip
of tape is used to cover the entrance of the crack. The fuel and oxi-
dizer flow rates are set to predetermined values. As the cold igniter
gases pass over the sealed crack entrance, a high-speed camera is turned
on. A timing signal is then activated which places light pulses on the
film and simultaneously sends a pulse to the tape recorder to synchro-
nize the film with the pressure data on the tape. Ignition is then
achieved with two conventional automobile spark plugs. Hot igniter-
gases pass from the igniter chamber through a multi-perforated nozzle to
the combustion chamber; the tape covering the crack entrance burns away
immediately and the hot gases enter the crack.

After an induction interval, the propellant at the crack entrance
reaches ignition condition. The flame spreading process is then observed
by the 16 mm high-speed camera. The pressurization process in the
propellant crack is simultaneously recorded on the magnetic tape.

DISCUSSION OF RESULTS

Calculations have been made with the present theoretical model to
compare with initial experimental data obtained from the crack combus-
tion facility. Additionally, a parametric study was conducted with the
theoretical model to ascertain the influence of variations in chamber
pressurizaton rate, crack gap width, and ignition parameters on the
flame spreading and resultant pressurization inside propellant cracks.

EXPERIMENTAL DATA AND THEORETICAL COMPARISON

A limited number of firings with a smokeless propellant have been
conducted in the newly developed crack combustion facility. The propel-
lant used in these firings was furnished by NWC. As described earlier

in this report, two different crack geometries have been tested. The larger crack ($\delta = 0.5$ cm) was used during the phase of initial system checkout and will be retested for documentation in a later report. The experimental results of a smaller crack, having a length of 15 cm and a gap width of 0.051 cm at the entrance with a gradual increase to 0.107 cm at the tip, are discussed herein. (Although we call the above configuration a "small" crack, the gap width may be an order of magnitude larger than that of the actual cracks found in rocket grains.)

Typical pressure-time traces recorded from a test firing of a "small" crack configuration are shown in Figure 8. G2 represents the pressure history at the entrance of the crack. G5 was initially covered by the propellant specimen and therefore senses pressure at a later time. In this test a large exhaust nozzle was used to produce a relatively low pressurization rate at the crack entrance. This resultant pressurization rate is close to the typical value obtained during the starting transient of many rocket motors. An examination of the G2 through G4 pressure-time traces reveal that the spatial pressure gradient inside the crack is very low. This nearly uniform spatial pressure history is due to the relatively low value of dPc/dt and to a significantly large gap width; these conditions are favorable for the reduction of pressure wave phenomena. As shown in Figures 9 and 10, the predicted P-t profiles at two stations inside the crack are in close agreement with the experimental data.
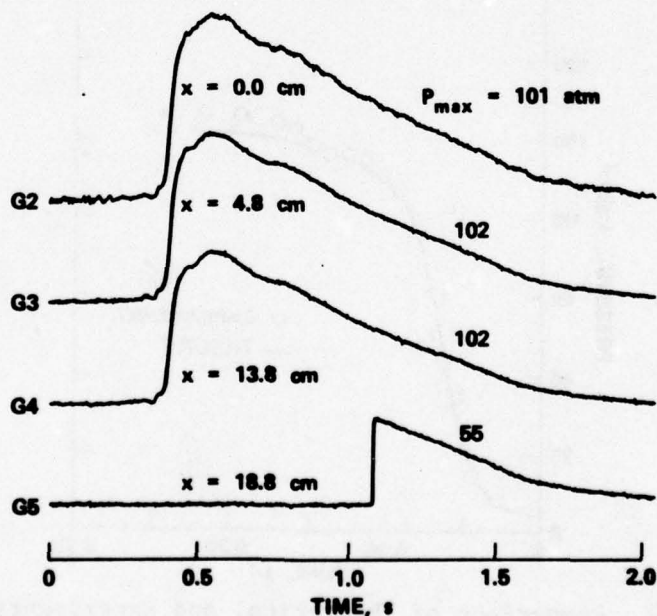
FIGURE 8. Experimental Pressure-Time Traces from DNC Test No. 11.
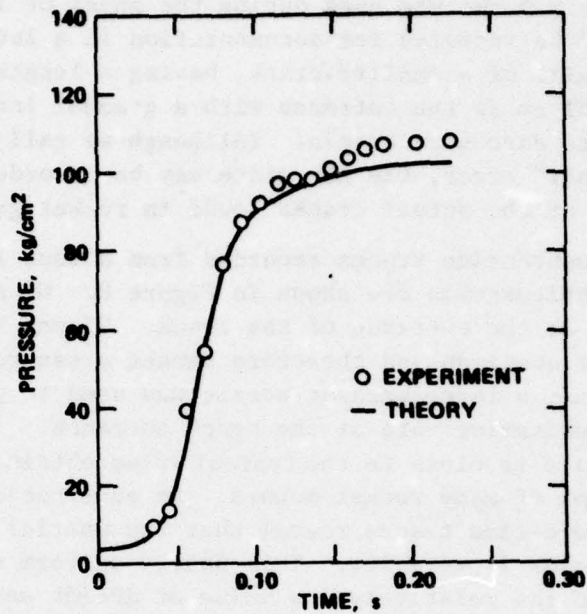
27

FIGURE 9. Comparison of Theoretical and Experimental P-t
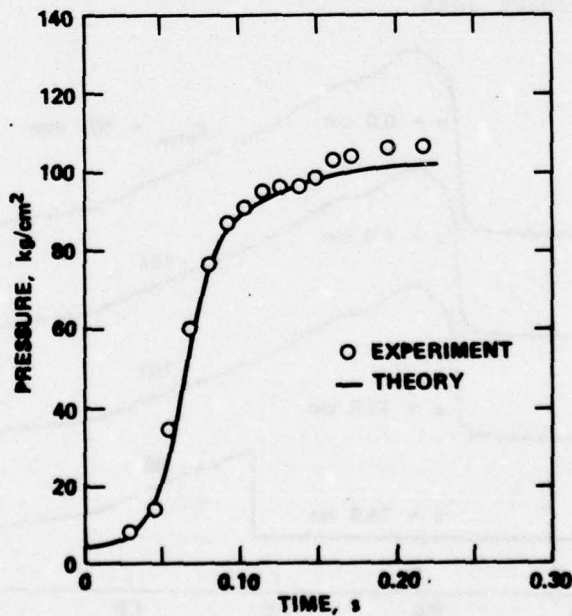Profiles at x = 4.8 cm (Simulation of DNC Test No. 11).

FIGURE 10. Comparison of Theoretical and Experimental P-t
Profiles at x = 13.8 cm (Simulation of DNC Test No. 11).

In this test an exceedingly long induction period was required for the igniter gases to burn away the protective tape and establish igni- tion at the crack entrance. Consequently, no useful flame spreading data was obtained. However, in another firing with nearly identical test conditions, the luminous flame front was found to propagate slowly near the crack entrance and then suddenly accelerate to a nearly uniform velocity. The film showing the characteristic features of the flame spreading process was presented at the last High Energy Propellant Safety (HEPS) Meeting held at NSWC/WOL, December 1976. A similar be- havior in the flame spreading rate was also observed experimentally by Balyaev.[6]

Figure 11 describes the calculated gas temperature distribution along the crack at various times. Because of the high flame temperature and short transient times, no attempt was made to measure the gas tem- perature inside the crack. The input data used to make these predic- tions are listed in Table 1. The locus of the calculated ignition front is superimposed on this figure. The gradient in the temperature distri- bution is very pronounced indicating the penetration of hot gases into the propellant crack. For times greater than 50 ms, the gas temperature at the opening portion of the crack decreases slightly; this is mainly due to the outflow of product gases.
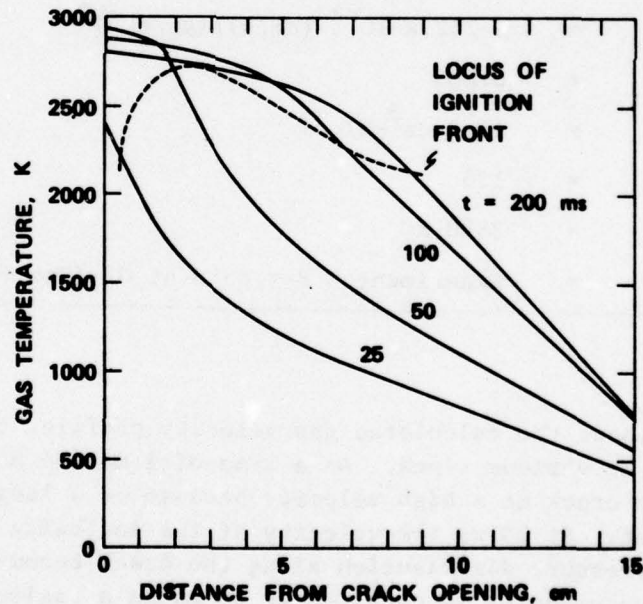
FIGURE 11. Calculated Gas Temperature Distribution for Various Times (Simulation of DNC Test No. 11).

TABLE 1. Computer Program Input Variable.

x_p	=	0.0 cm
x_L	=	15.05 cm
B_x	=	0.0 g_f/g
b	=	1.0 cm^3/g
M_w	=	23.97 g_f/g-mole
γ	=	1.233
ρ_{pr}	=	1.741 g/cm^3
γ_{pr}	=	0.44 x 10^{-3} cal/s-cm-K
α_{pr}	=	0.001 cm^2/s
ε_s/d_h	=	0.001
T_f	=	3000 K
T_{cri}	=	780 K
T_{ign}	=	1000 K
T_i	=	298 K
a	=	2.752 x 10^{-4} (cm/s)/$(g_f/cm^2)^n$
n	=	0.683
K_e	=	15.9 cm^3-K/cal
β	=	125
T_c	=	2800 K
P_c	=	Experimental P-t data at G2 (See Figure 8)

Figure 12 shows the calculated gas velocity profiles that exist in the small crack at various times. At a time of 1 ms the hot gases are flowing into the crack at a high velocity because of a large initial pressure gradient. At 25 ms the velocity of the inflowing gases decreases as the pressure distribution along the crack becomes more uniform. A negative velocity is obtained at 50 ms in a region near the crack opening which indicates an outflow of product gases. As the flame front progresses along the crack, the resultant gasification processes
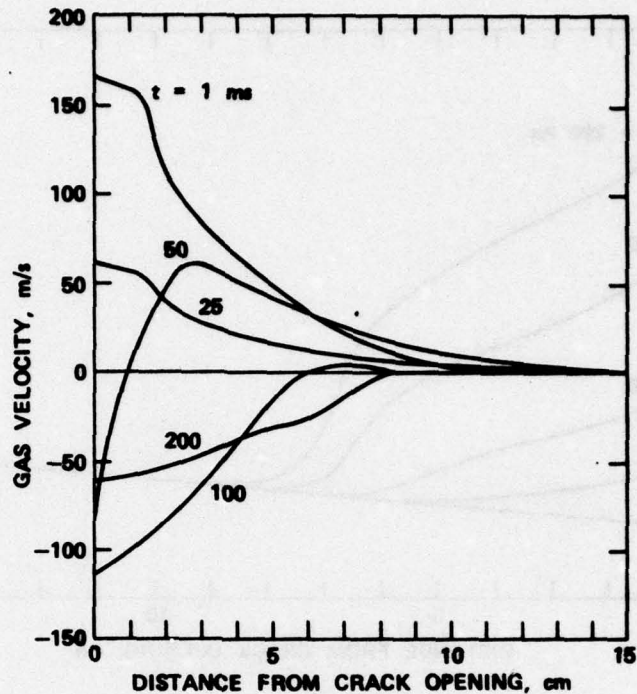
30

FIGURE 12. Calculated Velocity Distribution at
Various Times (Simulation of DNC Test No. 11).

cause an increase in velocity of the gases flowing out of the crack.
Due to the large increase in port area at opening of the crack (see
Figure 13), the velocity of the out-flowing gases decreases between 100
and 200 ms. During the entire pressurization process, the gas velocity
near the closed end of the crack is very low; this is due to the lack of
a favorable pressure gradient. This very low flow velocity causes a
significant reduction in the convective heating of the propellant sur-
face. Hence, a much longer time is required for the propellant surface
near the crack tip to achieve a state of ignition. This delay is readily
evident in the calculated flame front propagation shown in Figure 14.

PARAMETRIC STUDY

A parametric study was conducted with the theoretical model to
determine the influence of variations in chamber pressurization rate,
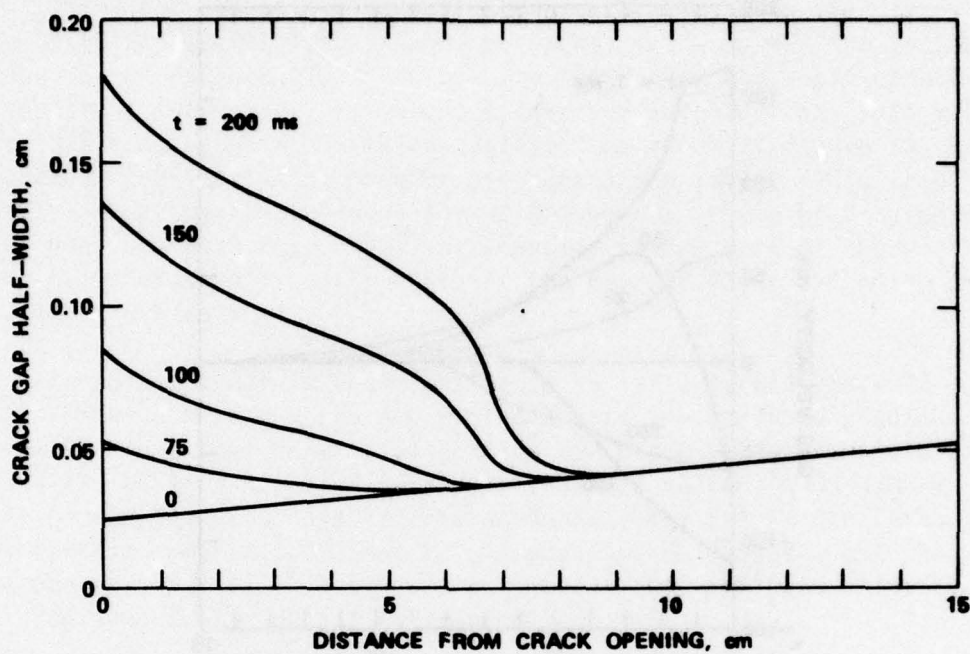crack gap width, and ignition parameters on the flame spreading and

31

FIGURE 13.   Calculated Growth of Crack Gap Due to
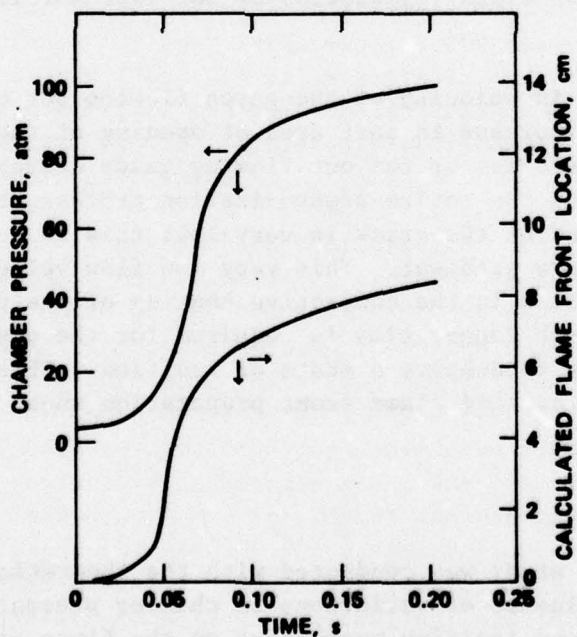Combustion (Simulation of DNC Test No. 11).

FIGURE 14.   Time Variation of Chamber Pressure
and Calculated Flame Front Location in DNC Test No. 11.

32

resultant pressurization inside propellant cracks. Unless otherwise described, the input constants used in this theoretical study are given in Table 1.

Figure 15 describes the pressure history at the tip of a small, constant area crack ($\delta = 0.02$ cm) for various chamber pressurization rates. Three sets of curves are shown in this plot for dP_c/dt varying from 0.5×10^4 to 1.5×10^4 atm/s. Each set of curves compares the calculated pressurization history at the tip of the crack with the assumed chamber pressure variation. These assumed chamber pressurization rates are of the same order of magnitude that a crack would experience during the starting transient of a rocket motor. As shown in this plot, the pressurization rate at the tip of the crack changes abruptly due to the gasification of propellant surface inside the crack. The time required to attain this "rapid pressurization" is aptly designated at t_{RP}.
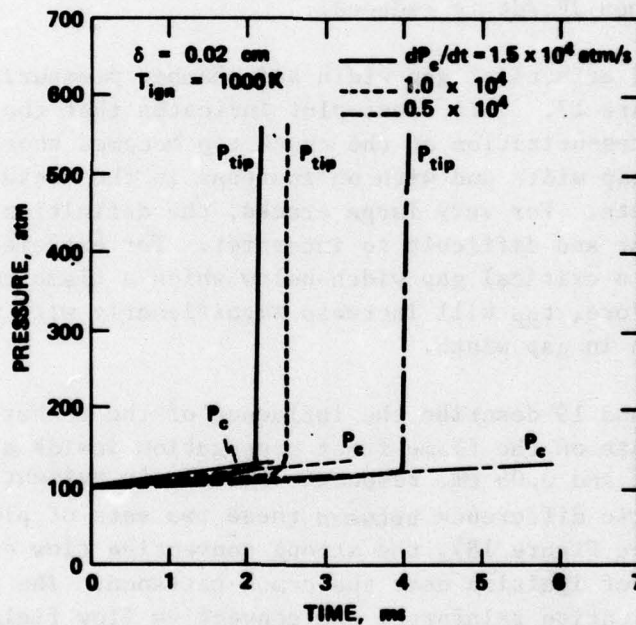

FIGURE 15. Influence of Rocket Chamber Pressurization Rate on the Internal Pressurization Process Inside a Narrow Crack ($\delta = 0.02$ cm).

33

This time can either be defined as: the time when the pressure at the crack tip exceeds the chamber pressure, or; when the two tangent lines, drawn on each side of the curve describing the rapid pressure transition, intersect. For small cracks and large dPc/dt, both methods for obtaining t_{RP} are nearly equivalent. As shown in Figure 15, t_{RP} decreases for increasing chamber pressurization rates. This trend is mainly due to the increase of forced convection driven by a large stream-wise pressure gradient. This augmentation in the rate of convective heat transfer significantly enhances the rate of flame spreading and surface gasification.

A similar study is shown in Figure 16 for a larger crack (δ = 0.05 cm). Because of the large gap width, a very low pressure gradient prevails along the crack. This causes the crack tip pressure to closely track the chamber pressure before appreciable surface gasification. For this particular case, t_{RP} is more adequately defined by the tangent-intersection method. Similar to the small crack results, the theoretical predictions for this large crack reveal that a larger delay in t_{RP} is experienced when dPc/dt is reduced.

The combined effects of gap width and chamber pressurization rate are shown in Figure 17. This cross-plot indicates that the time required to reach rapid pressurization at the crack tip becomes shorter with a decrease in the gap width and with an increase in the rocket chamber pressurization rate. For very large cracks, the definition of t_{RP} becomes less clear and difficult to interpret. For extremely small cracks, there is a critical gap width below which a flame cannot easily propagate; therefore, t_{RP} will increase significantly with a further reduction in gap width.

Figures 18 and 19 describe the influence of the rocket chamber pressurization rate on the flame front propagation inside a crack with a gap width of 0.02 and 0.05 cm, respectively. It is evident that there is a characteristic difference between these two sets of plots. For the smaller crack (see Figure 18), the strong convective flow enhances an early attainment of ignition near the crack entrance. The resultant propellant gasification reinforces the convective flow field and causes the flame front to rapidly accelerate along the crack. For distances along the crack less than 5 cm, the rocket chamber pressurization rate significantly affects the rate of flame propagation. However, for x > 5 cm, the flame front propagation velocity (approximately 800-900 m/s) is dominated by interior propellant gasification, and the influence of the rocket chamber pressurization is diminished; therefore, the slopes of

34
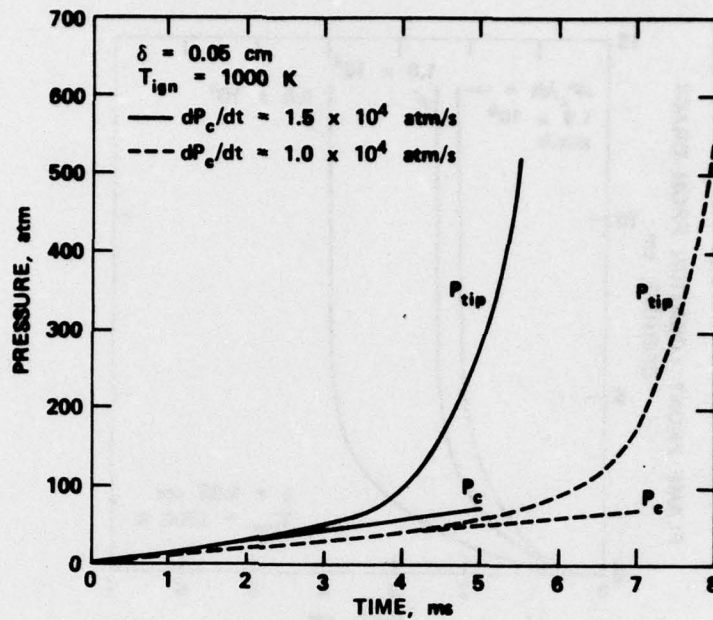
FIGURE 16.   Influence of Rocket Chamber Pressurization Rate on the
Internal Pressurization Process Inside a Wide Crack (δ = 0.05 cm).

FIGURE 17.   Influence of Gap Width and Rocket Chamber Pressurization
Rate on the Time to Reach Rapid Pressurization at Crack Tip.

35

FIGURE 18.   Influence of Rocket Chamber Pressurization Rate on
the Flame Spreading Inside a Narrow Crack (δ = 0.02 cm).
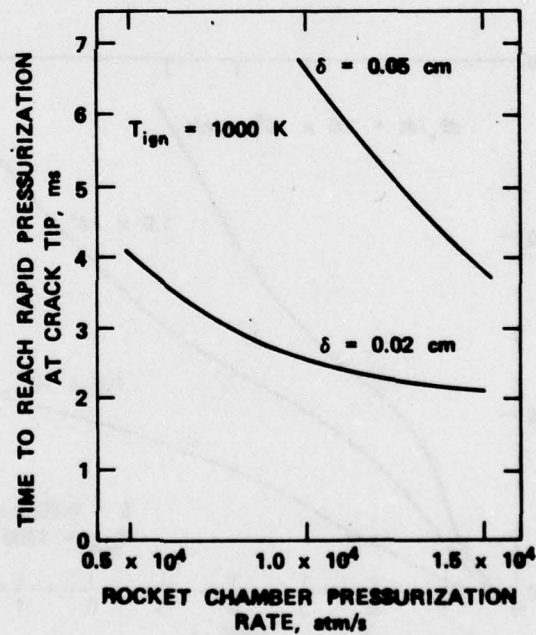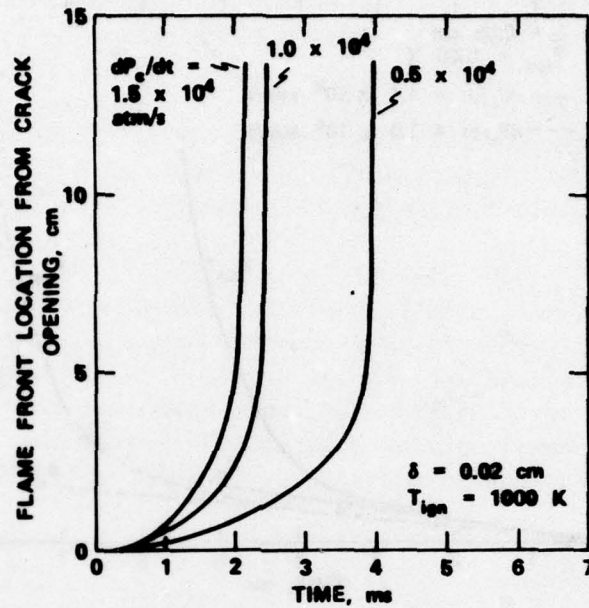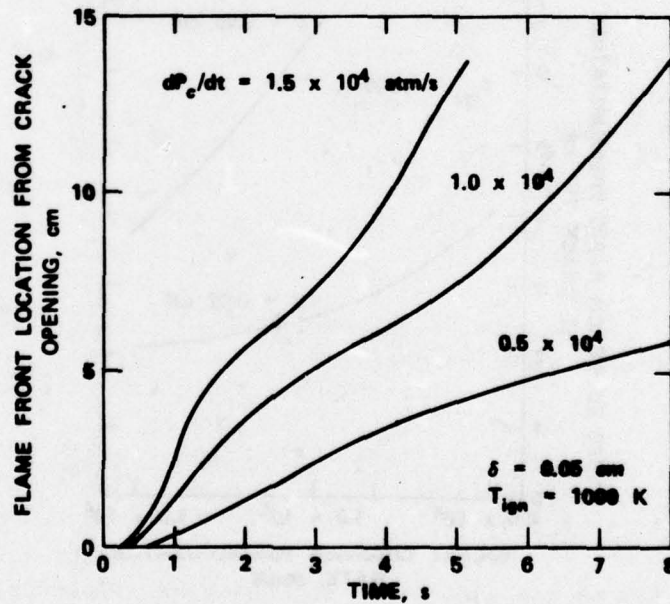

FIGURE 19.   Influence of Rocket Chamber Pressurization Rate
on the Flame Spreading Inside a Wide Crack (δ = 0.05 cm).

36

these curves are approximately the same. For the larger crack (see Figure 19), the rocket chamber pressurization rate and the local gasification processes are both important factors controlling the rate of flame propagation and, as discussed earlier, the pressure at the crack tip.

The influence of propellant ignition temperature on the time to reach rapid pressurization at the crack tip, t_{RP}, is shown in Figure 20 for various rates of rocket chamber pressurization. It is found that t_{RP} for this small crack ($\delta = 0.02$ cm) diminishes with a reduction in the ignition temperature. Also, the slope of t_{RP} versus T_{ign} decreases as the chamber pressurization rate increases. This implies that the flame spreading and pressurization processes inside a crack of a given initial geometry become less sensitive to the propellant ignition temperature as the forced convection becomes stronger.
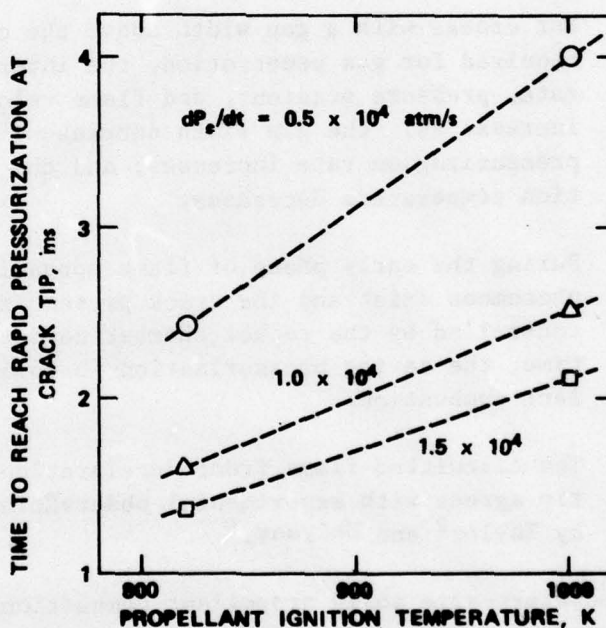

FIGURE 20. Influence of Propellant Ignition Temperature and Rocket Chamber Pressurization Rate on the Time to Reach Rapid Pressurization at Crack Tip.

37

SUMMARY OF PROGRESS AND CONCLUSIONS

The experimental and theoretical progress achieved at Pennsylvania State University in understanding the complicated combustion processes that occur in a single, isolated, propellant crack is summarized in the following.

1. A one-dimensional theoretical model, incorporating the Noble-Abel dense gas law, has been developed to describe the transient combustion phenomena in a propellant crack. The theoretical model can be used to predict wave phemomena, heat transfer from the gas to the propellant surface and associated thermal penetration, flame propagation and resultant pressurization at various locations along the propellant cavity.

2. Several important results of the theoretical study are listed below.

    a. For cracks with a gap width above the critical value required for gas penetration, the internal pressurization rate, pressure gradient, and flame velocity in the crack increase as: the gap width decreases; the rocket chamber pressurization rate increases; and the propellant ignition temperature decreases.

    b. During the early phase of flame spreading, pressure wave phenomena exist and the crack pressurization rate is controlled by the rocket chamber conditions. At a later time, the cavity pressurization is dominated by propellant combustion.

    c. The calculated flame front deceleration near the crack tip agrees with experimental observations made separately by Taylor[2] and Belyaev.[6]

3. A laboratory-size solid propellant combustion chamber has been designed, fabricated, and tested. A series of firings with single-pore propellants has been conducted for initial system checkout.

4. Preliminary experimental data, obtained in wide cracks ($\delta \sim 0.1$ cm) for relatively low chamber pressurization rates, are in agreement with theoretical predictions.

NOMENCLATURE

A_p Cross-sectional area of the crack, cm^2

A_{px} Spatial change of cross-sectional area of crack with respect to the axial distance, cm

a Pre-exponential factor in the nonerosive burning rate law, ap^n, $(cm/s)(cm^2/g_f)^n$

B_x Body force, g_f/g

b Co-volume, cm^3/g

c Speed of sound, cm/s; when with subscript, specific heat, cal/g-K

c_f Friction coefficient, $2g\pi_w/\rho u^2$

c_p Specific heat at constant pressure, cal/g-K

d_h Hydraulic diameter of the crack, cm

E Total stored energy (internal and kinetic), cal/g

g Acceleration of gravity, conversion factor, $g\text{-}cm/g_s\text{-}s^2$

H Depth of the gap in flow visualization tests, cm

$\bar{h}_c$ Local convective heat-transfer coefficient, $cal/cm^2\text{-}s\text{-}K$

$\bar{h}_{cp}$ Local convective heat-transfer coefficient over the propellant surface, $cal/cm^2\text{-}s\text{-}K$

$\bar{h}_{cw}$ Local convective heat-transfer coefficient over non-propellant port wall, $cal/cm^2\text{-}s\text{-}K$

h_f Enthalpy of combustion gas at adiabatic flame temperature, cal/g

J Mechanical equivalent of heat, $g_f\text{-}cm/cal$

K_e Erosive burning constant, $cm^3\text{-}K/cal$

L Length of the crack, cm

M_w Molecular weight, $g_f/g\text{-}mole$

n Pressure exponent in the non-erosive burning rate law

Pr Prandtl number

$\mathscr{P}_b$ Burning perimeter, cm

$\mathscr{P}_w$ Wetted perimeter of the port, cm

P Static pressure, g_f/cm^2
(or p)

R Specific gas constant for the combustion gases, $g_f\text{-}cm/g\text{-}K$

Re Reynolds number

r_b Burning rate of the solid propellant, including the erosive burning contribution, cm/s

T Temperature (without subscript, static gas temperature), K

T_{af} Average film gas temperature $(T + T_{ps})/2$, K

T_f Adiabatic flame temperature of the solid propellant, K

T_{pi} Initial propellant temperature, K

T_{ps} Propellant surface temperature, K

T_{ws} Nonpropellant wall surface temperature, K

t

u

V_{gf}

V_k

x

x_L

x_p

y

Symb

δ

α

β

γ

ϵ

ϵ_s

λ

μ

ρ

τ_w

τ_{xx}

θ_w

Subs

c

cri

i

ign

pr

RP

tip

3

t	Time, s
u	Gas velocity, cm/s
V_{gf}	Velocity of propellant gas at the burning surface, cm/s
V_k	Coefficient in viscosity-temperature relation
x	Axial distance from propellant crack opening, cm
x_L	Position at the end of crack, cm
x_p	Axial distance along the crack at which propellant begins, cm
y	Perpendicular distance from the propellant surface into the solid, cm

Symbols

δ	Gap width of the crack, cm
α	Thermal diffusivity, cm^2/s
β	Erosive burning exponent
γ	Ratio of specific heats
ε	Small number of K
ε_s	Surface roughness, cm
λ	Thermal conductivity, cal/cm-s-K
μ	Gas viscosity, g/cm-s (poise)
ρ	Density (without subscript, gas density), g/cm^3
τ_w	Shear stress on the port wall, g_f/cm^2
τ_{xx}	Normal viscous stress, g_f/cm^2
θ_w	Angle measured, in a counterclockwise direction, at the lower side of the propellant, degree

Subscripts

c	Rocket chamber
cri	Critical condition for surface ablation
i	Initial value
ign	Ignition condition
pr	Propellant
RP	Rapid pressurization
tip	Crack tip

INITIAL DISTRIBUTION

1 Director of Navy Laboratories
8 Naval Air Systems Command
    AIR-30212 (2)
    AIR-330 (1)
    AIR-330B, Robert H. Heitkotter (1)
    AIR-330D (1)
    AIR-536 (1)
    AIR-954 (2)
4 Chief of Naval Operations
2 Chief of Naval Material
    MAT-03 (1)
    MAT-03PB (1)
7 Naval Sea Systems Command
    SEA-03 (1)
    SEA-033 (1)
    SEA-0331, Murrin (1)
    SEA-0331B, Cassel (1)
    SEA-0332 (1)
    SEA-09G32 (2)
7 Chief of Naval Research, Arlington
    ONR-100 (1)
    ONR-102 (1)
    ONR-401 (1)
    ONR-420 (1)
    ONR-472 (1)
    ONR-473 (1)
        James R. Patton, Jr. (1)
2 Naval Ordnance Station, Indian Head
    Code FS71C, Alan Roberts (1)
    Technical Library (1)
3 Naval Postgraduate School, Monterey
    Code 57, Fuhs (1)
    Code 57NT, Netzer (1)
    Technical Library (1)
3 Naval Research Laboratory
    Code 2021 (1)
    Code 6130, Chemistry Division (1)
    Technical Library (1)
1 Naval Underwater Systems Center, Newport (Code 5B331, Robert S. Lazar)
1 Naval Weapons Evaluation Facility, Kirtland Air Force Base (Code 401)

41

2 Navy Stratetic Systems Project Office
   SP-2731, Roy Kinert (1)
   NSP-2731, Throckmorton (1)
1 Army Material Development & Readiness Command (AMCRD-WM,
   Stephen R. Matos)
1 Army Missile R&D Command, Redstone Arsenal (AMSMI-RK, Donald J. Ifshin)
1 Army Armament Research & Development Center (SMUPA-TS-TS, J. Picard)
2 Army Ballistic Research Laboratories, Aberdeen Proving Ground
   AMXBR-IB
      Austin W. Barrows (1)
      Ingo W. May (1)

1 Rock Island Arsenal (Edward Haug)
1 Air Force Armament Laboratory, Eglin Air Force Base
   (DLDL, Otto K. Heiney)
1 Air Force Rocket Propulsion Laboratory, Edwards Air Force Base
   (DYSC, Wilbur C. Andrepont)
1 Bolling Air Force Base (NA, Thomas C. Meier)
12 Defense Documentation Center
1 National Aeronautics & Space Administration (Code RP,
   Frank W. Stephenson, Jr.)
2 George C. Marshall Space Flight Center
   SE-ASTN-PEA, John Q. Miller (1)
   Richard J. Richmond (1)
1 Lewis Research Center (Richard J. Priem)
1 Lyndon B. Johnson Space Center (EP, Joseph G. Thibodaux)
1 Aerojet Solid Propulsion Company, Sacramento, Calif. (Dept. 4350,
   Arthur L. Karnesky) via AFPRO
1 Aerospace Corporation, Los Angeles, Calif. (Ellis M. Landsbaum)
1 Allegany Ballistic Laboratory, Cumberland, Md. (Roy R. Miller)
1 Atlantic Research Corporation, Alexandria, Va. (Merrill K. King)
1 Battelle Memorial Institute, Columbus, Ohio (Abbott A. Putman)
1 Brigham Young University, Provo, Utah (673/W1DB, L. Douglas Smoot)
1 California State University Sacramento, Sacramento, Calif.
   (School of Engineering, Frederick H. Reardon)
1 Calspan Corporation, Buffalo, N.Y. (Edward B. Fisher)
1 Chemical Propulsion Information Agency, Applied Physics Laboratory,
   Laurel, Md. (Thomas W. Christian)
3 Georgia Institute of Technology, Atlanta, Ga.
   Ben T. Zinn (1)
   Edward W. Price (1)
   Warren C. Strahle (1)
2 Hercules Incorporated, Bacchus Works, Magna, Utah
   Merrill W. Beckstead (1)
   Ronald L. Simmons (1)
2 Jet Propulsion Laboratory, Pasadena, Calif.
   Fred E. C. Culick (1)
   Leon D. Strand (1)

25 Pennsylvania State University, University Park, Pa.
 1 Princeton University Forrestal Campus Library, Princeton, N.J.
   (Leonard H. Caveny)
 1 Propulsion Sciences Incorporated, Melville, N.Y. (Vito Agosta)
 1 Purdue University, West Lafayette, Ind. (School of Mechanical
   Engineering, John R. Osborn)
 2 Rockwell International Corporation, Canoga Park, Calif.
     Dept, 589-197-SS11, Carl L. Oberg (1)
     Joseph E. Flanagan (1)
 1 Rockwell International Corporation, McGregor, Tex. (William G. Haymes)
 1 Shock Hydrodynamics Incorporated, Sherman Oaks, Calif.
   (W. H. Anderson)
 1 Southwest Research Institute, San Antonio, Tex. (Fire Research Section,
   William H. McLain)
 1 TRW Systems Inc., Redondo Beach, Calif. (A. C. Ellings)
 1 Thiokol Corporation, Huntsville Division, Huntsville, Ala.
   (David A. Flanigan)
 1 Thiokol Corporation, Wasatch Division, Brigham City, Utah
   (John A. Peterson)
 1 United Technologies Corporation, East Hartford, Conn. (R. H. W. Waesche)
 1 United Technologies Corporation, Sunnyvale, Calif. (Chemical Systems,
   Division, Robert S. Brown)
 1 University of California, San Diego, La Jolla, Calif. (AMES Dept.,
   Forman A. Williams)
 1 University of Illinois, Urbana, Ill. (AAE Department, Herman Krier)
 1 University of Massachusetts, Amherst, Mass. (Dept. of Mechanical
   Engineering, Karl Jakus)
 1 University of Utah, Salt Lake City, Utah (Dept. of Chemical Engineering,
   Alva D. Baer)
 1 Whittaker Corporation, Bermite Division, Saugus, Calif. (J. Hammond)

NT.